PCCP

Accepted Manuscript

ROYAL SOCIETY OF CHEMISTRY

www.rsc.org/pccp

PCCP

RSCPublishing

COMMUNICATION

Urchin-like TiO_2@C core-shell microspheres: coupled synthesis and lithium-ion battery applications

Cite this: DOI: 10.1039/x0xx00000x

Zhenyu Liu,[ac‡] Jing Liu,[a‡] Junfeng Liu[a], Li Wang,[b*] Guoxin Zhang[a] and Xiaoming Sun[*a]

Received 00th January 2012,
Accepted 00th January 2012

DOI: 10.1039/x0xx00000x

www.rsc.org/

Carbon coated urchin-like TiO_2 microspheres were prepared through coupled hydrolysis of titanium tetrachloride and catalyzed carbonization of glucose. Carbon coating endowed the composite with unusual structure stability at high temperature and reasonable Li ion battery performance.

Titanium dioxide (TiO_2), as an abundant, low cost, and environmentally friendly material, has been widely studied for its wide applications, such as lithium-ion batteries (LIB), solar cells, sensors, and photocatalysts.[1-6] As anode materials for LIB, TiO_2 shows superior safety compared to graphite.[7] But its poor electron transport and lithium ion diffusivity hinder its applications. Reducing the particle size of TiO_2 to nano-meters could benefit both power rate and cycling performance by providing short pathway for electron and lithium ion transport, increasing high electrode–electrolyte contact area, and accommodating the strain during Li insertion/extraction.[8, 9] In recent years, coating the electrochemically reactive oxide with carbonaceous material and assembling nanosized particles into three-dimensional (3D) superstructures[10-19] is proved an ideal strategy for insulating material to obtain both high tap density and good electrochemical performances.[20] However, to assemble TiO_2 3D nanostructures with carbon nanomaterials in a regular way remains a challenge. More importantly, the carbonaceous materials need high temperature to increase the graphitization and the conductivity, while the TiO_2 nanoparticles would grow and lose the size effect during annealing process.

In previous research, oxide@C core-shell nanostructures were prepared by coupled hydrolysis of metal salts and carbonization of glucose.[21-23] Aqueous media was usually used because it is a good solvent for both, but $TiCl_4$'s hydrolyzation happens too fast to be coupled with dehydration of glucose. Inspired from a TiO_2 nanoparticle synthesis method,[24] which took place in alcohol media and used esterification to deliver water molecules for hydrolysis and control the sizes of final particles, we introduced glucose to the esterification system and realized coupled dehydration of glucose and growth of TiO_2 nanorods. The resultant urchin-like microspheres are assembled from TiO_2 nanorods with only ~10 nm diameter radically grown from the centre, with all the inter-rod spaces filled with carbon. The synergistic growth of TiO_2 nanorods and coating nanocarbon endowed the composite with superior thermal stability and electrochemical performance as Li-ion battery electrode.

For the solvothermal synthesis, $TiCl_4$ was dissolved in alcohol to form a clear solution, then acetate acid was added by a molar ratio of alcohol : acetate = 2 : 1. As the system was heated to 140 - 180 ^oC, both the esterification and the glucose dehydration took place and delivered water. The water delivered was used for $TiCl_4$ hydrolysis to form TiO_2. As-formed carbon coated certain facets of TiO_2 nano-crystals and led to oriented growth, which resulted in formation of nanorods. As these nanorods' growth started from one nuclei centre, a composite TiO_2@C microspheres formed with diameters ranged from 1 to 10 μm (Fig.1a). The high-magnification SEM image shown in Fig. 1b highlighted the coarse surface of a microsphere, where lots of "thorns" exist (Fig. 1c and Fig. S1). The cross-sectional view revealed the radiated growth of the nanorods. Crystal structure of the nanorods was then examined by HRTEM analysis together with the corresponding fast Fourier transform (FFT) patterns (Fig. 1d). The distance between adjacent lattice fringes that run parallel to the nanorod wall were 3.23 Å, which was assigned to the interplane distance of (110) planes in the rutile structure of TiO_2. The distance between the fringes perpendicular to the wall, (*i.e.*, d = 2.97 Å) was in agreement with the lattice spacing of rutile (001) planes. The two observations indicated that the nanorods grew along *c*-axis. The thin amorphous carbonaceous layer coated on the TiO_2 nanorods was less than 2 nm in thickness, as revealed under TEM (Fig. 1d and Fig. S2).

The XRD pattern (Fig. 1e) of the as-prepared TiO_2@C material shows that the TiO_2 inside is a mixed phase of rutile (JCPDS No. 21-1276) and anatase (JCPDS No. 21-1272), which is also in accord with the Raman spectra presented in Fig. 1f. The peak at 142 cm^{-1} and a minor peak at 512 cm^{-1} are consistent with the presence of the anatase phase of TiO_2 (The two lower lines are the standard curves of rutile and anatase TiO_2). And the peaks at 234, 439 and 612 cm^{-1} are assigned to the presence of the rutile phase of TiO_2.[1, 25] The peaks at 1359 and 1605 cm^{-1} are attributed to the D band (disorderd)

and G band (graphitic) of carbon respectively, which evidenced the existence of carbon.

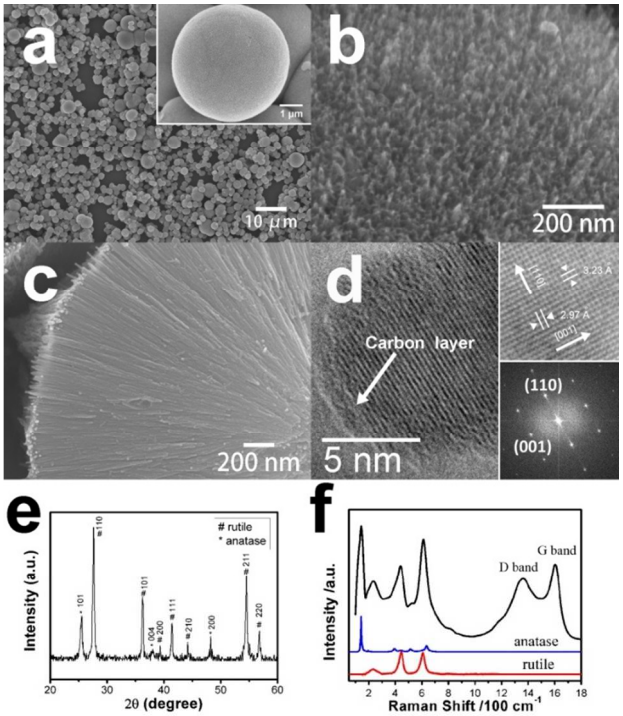

Fig. 1 TiO_2@C microspheres prepared with 1 g glucose at 140 °C before annealing: (a) Low magnification SEM images (inset: a high magnification of an individual sphere), (b) surface and (c) cross-sectional SEM images. (d) HRTEM image and Fourier transform pattern of a TiO_2 nanorod. (e) XRD pattern and (f) Raman spectra of the TiO_2@C microspheres.

To ensure that the carbon was encapsulating TiO_2 nanorods and the amorphous layer in Fig.1d was not oxide, the calcined sample was treated with 47% HF solution under sonication for 4 h to remove TiO_2 components. The remaining black substance could be well dispersed even for several hours without visible aggregation. The morphology of the residue was characterized by SEM. Porous carbon spheres were observed in the SEM image (Fig. 3a and b). The centres of the spheres were hollow, suggesting hydrolysis of $TiCl_4$ happened before dehydration of glucose, so the TiO_2 initially formed have little carbon coating. As the reaction time extended, carbonization of glucose took place and resulted in the formation of carbon on the surface of TiO_2. The diameters of the tube-like pores were tens of nanometer, much larger than the diameter of a single TiO_2 nanorod, which might be due to the collapse of thin carbon layer during sonication.

Hydrothermal temperature was crucial to the carbonization of glucose.[26] It could be also confirmed in this work. TiO_2@C microspheres were prepared at different temperatures, and their corresponding SEM images are shown in Fig. 2. TiO_2 nanorods in the microspheres prepared at 80 ˚C had a diameter of 40 – 50 nm (Fig. 2a), thicker than those obtained at 100 ˚C, which were about 30 nm in diameter (Fig. 2b). As the hydrothermal temperature was increased to 120 ˚C or higher, the sizes of the nanorods reduced to 10 – 20 nm and the intensity of rutile phase became stronger (Fig. S3). However, with further enhanced the reaction temperature, the nanorod diameters didn't show obvious shrinkage. It was considered that the carbon coating layers controlled the growth of the TiO_2 nanorods, so the nanorods couldn't grow big as long as the temperature is high enough to induce the carbonization of glucose. The carbonaceous layers bonded to the TiO_2 surfaces tightly due to the possible functional groups and acted as template to prevent its radial growth. That should be the reason why the TiO_2 in the microspheres prepared at higher temperatures kept their slim shapes with small diameters.

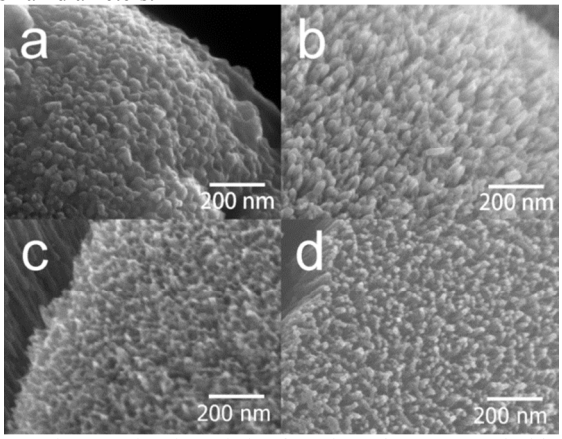

Fig. 2 SEM images of surface of TiO_2@C microspheres prepared with 1 g glucose at 80, 100, 120 and 180 ˚C (a, b, c and d respectively).

The TiO_2@C microspheres were annealed in Ar atmosphere at 700 ˚C for 2 h before Li-ion battery test because previous results have indicated that temperature higher than 650 °C was required for good crystallinity and electrical conductivity.[27, 28] Surprisingly, in contrast to previous reports that the phase transformation temperature for rutile TiO_2 was as low as 550 °C and such conversion would cause particle size growth,[25] the microsphere morphology was kept and the sizes of nanorods didn't increase much after annealing (Fig. 3c). It was believed that carbon coating isolated the individual TiO_2 nanorods and prevented sintering at high temperatures (Fig. S4). However, as the materials were treated at 500 ˚C for 3 h in air, and carbon was burned out completely (we can see the initial black materials turned white), the diameters of obtained nanorods TiO_2 (~60 nm) were much larger than those of nanorods (10 – 20 nm) before heat treatment (Fig. 1b). This change was attributed to the further growth of TiO_2 nanorods during the calcination without the confinement of carbon layer. It demonstrated that the carbon coating could effectively hinder the growth of TiO_2 nanorods when high temperature was required for high graphitization degree. Since the sizes of TiO_2 nanoparticles significantly affect their LIB performances,[29-32] good electrochemical performances of the as-prepared TiO_2@C can be expected. Nevertheless, the valences of Ti after heat treatment under inert atmosphere and air atmosphere were similar. (Fig. S5)

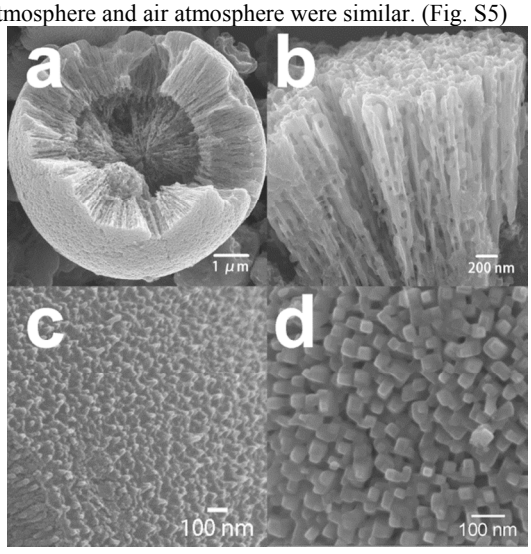

Fig. 3 SEM images of TiO_2@C microspheres: (a) and (b), etched by HF; (d), anealed at 700 ˚C under Ar protection; (c), anealed at 500 ˚C in air.

Before LIB test, we measured the weight ratio of carbon components of TiO_2@C microspheres using TGA measurements. The C content varied from 1.7% to 9%, depending on the amount of glucose introduced at hydrothermal step (from 0.25 to 1.0 g). Table S1 lists the products weight details according to the TGA results. It could be seen that the TiO_2 yield was increased as more glucose was added. This implied that the dehydration process of glucose was playing an important role in delivering water for hydrolysis of $TiCl_4$. This was supported by another fact that the carbon content also increased as the yield of TiO_2 increased.

As depicted in Fig. 3c and d, carbon layers significantly affected the sizes of TiO_2 nanorods during annealing, which may result in different LIB performances. The electrochemical reactivity of the TiO_2@C microspheres annealed at different temperatures was tested up to 90 cycles at a current of 30 $mA{\cdot}g^{-1}$. The influences of carbon layer on lithium ion storage capacity of TiO_2@C micropsheres were studied by limiting voltage window between 3 and 1 V, where the capacity contribution of carbon layer could be ignored. The 2nd cycle galvanostatic profiles of the TiO_2@C microspheres annealed in Ar (denoted as TiO_2@C-x, x stands for the annealing temperature) and air (denoted at TiO_2-air) were shown in Fig. 4a. The clear voltage plateau at about 1.75 V corresponded to lithium insertion into crystalline TiO_2. The electrochemical reversible reaction can be described as:

$$TiO_2 + xLi^+ + xe^- \longleftrightarrow Li_xTiO_2 \quad (1)$$

The theoretical charge storage capacity is 167.5 $mAh{\cdot}g^{-1}$ with the maximum insertion coefficient x determined to be ~0.5. The capacity of TiO_2@C-500 was only 55 and 36 $mAh{\cdot}g^{-1}$ for the 1st and 90th cycle, which may be attributed to the poor electronic conductivity of carbon layer. With the annealing temperature increasing, the carbon content didn't change (Tab. S2) but larger capacity was reached. The first discharge capacities of TiO_2@C-600, TiO_2@C-700, and TiO_2@C-800 were 169, 179, and 165 $mAh{\cdot}g^{-1}$, respectively (Fig. 4b). To our surprise, TiO_2-air, whose carbon component had been removed, had a discharge capacity of 202 $mAh{\cdot}g^{-1}$ in the first cycle, which might be due to its higher porosity caused by carbon removal. However, without carbon coating, its capacity dropped to 132 $mAh{\cdot}g^{-1}$ after 90 cycles (35% loss). In contrast, all carbon encapsulated samples showed much more stable performance, and higher temperature lead to higher stability. TiO_2@C-800 exhibited the best cycle performance and its discharge capacity retained at 143 $mAh{\cdot}g^{-1}$ after 90 cycles. This was attributed to the better crystallization of inner TiO_2 nanorods and higher graphitization degree, as the D/G ratio decreased with the increasing of annealing temperature (Fig. S6 and Tab. S3). Figure 4c presents the rate capability of these materials. The results show that the reversible capacity of TiO_2@C-800 at low rate was ~173 $mA{\cdot}g^{-1}$, similar to that of TiO_2-air. While at high rate, TiO_2-air exhibited better performances than these carbon-contained samples. When the current density is lowered to 20 $mA{\cdot}g^{-1}$ again, the specific capacity of TiO_2-air decreased to ~160 $mA{\cdot}g^{-1}$. However, capacity of ~172 $mA{\cdot}g^{-1}$ could be recovered for TiO_2@C-800, suggesting its good reversibility. These results indicated that carbon could significantly enhance the cycle stability, possibly due to its confined effect for TiO_2 volume change during Li^+ insertion/extraction.

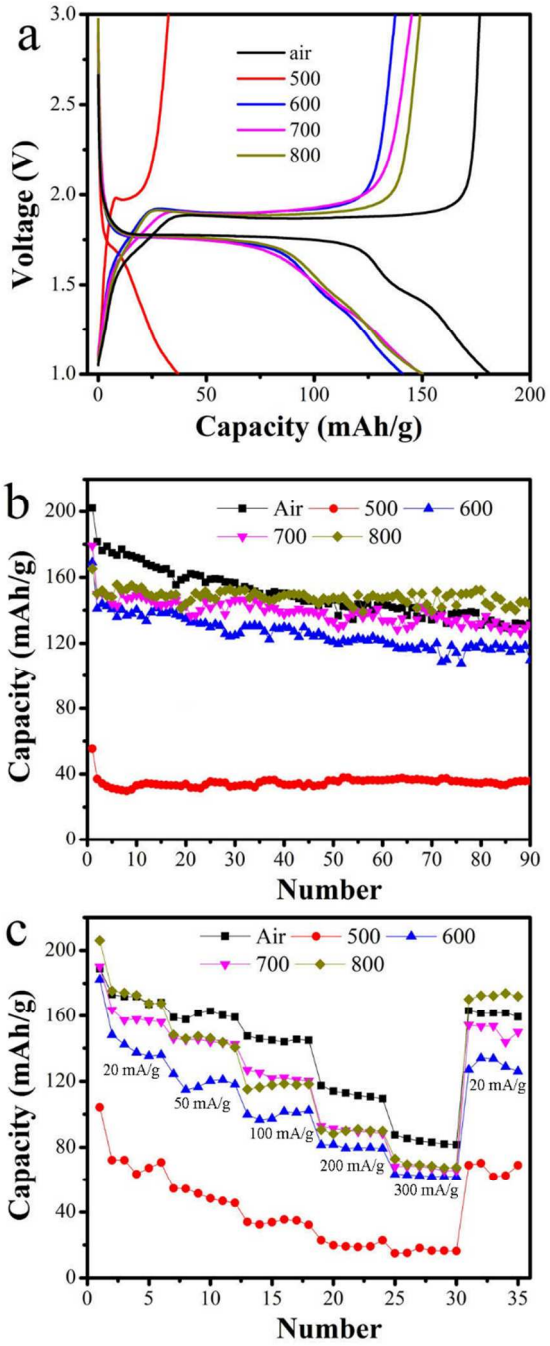

Fig. 4 Lithium ion storage performances of TiO_2@C microspheres annealed at different temperatures in Ar atmosphere and 500 ˚C in air: (a) 2nd cycle galvanostatic charge/discharge curves, (b) cyclic retention and (c) capacity at different charge/discharge current densities.

Conclusions

In summary, carbon coated urchin-like TiO_2 microspheres were synthesized via a facile one-step solvothermal method. The microspheres consisted of radically self-assembled TiO_2 nanorods and carbon homogeneously filled into the interspace of the nanorods to isolate them. The carbon formed an effective matrix for the individualized TiO_2 nanorods and prevented sintering of TiO_2 nanorods during the heat treatment. In LIB application, carbon component helped transfer electrons and stabilized the structure, and thus enhanced the cycling stability. This demonstrated the structural

optimization could provide new opportunities for enhancing the properties of solids in nanoscale.

Acknowledgements

This work was supported by National Natural Science Foundation of China, the 973 Program (2011CBA00503, 2011CB935902, 2010DFA72760, 2011CB932403) and the Program for New Century Excellent Talents in Universities, the Program for Changjiang Scholars and Innovative Research Team in University.

Notes and references

[a] *State Key Laboratory of Chemical Resource Engineering, Beijing University of Chemical Technology, Beijing 100029, China. Email: sunxm@mail.buct.edu.cn*

[b] *Institute of Nuclear and New Energy Technology, Tsinghua University, Beijing 100084, China. E-mail: wang-l@mail.tsinghua.edu.cn*

[c] *Maoming Branch R&D Institute, SINOPEC, Maoming 525011, China*

† Electronic Supplementary Information (ESI) available: Experimental details, supplementary figures and and tables as mentioned in the text. See DOI: 10.1039/c000000x/

‡ contributed equally to this work

1. X. Chen and S. S. Mao, *Chem. Rev.*, 2007, **107**, 2891-2959.
2. J. Maier, *Nat Mater*, 2005, **4**, 805-815.
3. W. J. Macklin and R. J. Neat, *Solid State Ionics*, 1992, **53-56**, 694-700.
4. G. Wang, X. Wang, J. Liu and X. Sun, *Chem. Eur. J.*, 2012, **18**, 5361-5366.
5. D. V. Bavykin, J. M. Friedrich and F. C. Walsh, *Adv. Mater.*, 2006, **18**, 2807-2824.
6. H. Y. Zhu, Y. Lan, X. P. Gao, S. P. Ringer, Z. F. Zheng, D. Y. Song and J. C. Zhao, *J. Am. Chem. Soc.*, 2005, **127**, 6730-6736.
7. G. Armstrong, A. R. Armstrong, P. G. Bruce, P. Reale and B. Scrosati, *Adv. Mater.*, 2006, **18**, 2597-2600.
8. H.-G. Jung, C. S. Yoon, J. Prakash and Y.-K. Sun, *J. Phys. Chem. C*, 2009, **113**, 21258-21263.
9. G. Du, Z. Guo, P. Zhang, Y. Li, M. Chen, D. Wexler and H. Liu, *J. Mater. Chem.*, 2010, **20**, 5689-5694.
10. H. Zhang, H. Yu, Y. Han, P. Liu, S. Zhang, P. Wang, Y. Cheng and H. Zhao, *Nano Res.*, 2011, **4**, 938-947.
11. Z. Sun, J. H. Kim, Y. Zhao, F. Bijarbooneh, V. Malgras, Y. Lee, Y.-M. Kang and S. X. Dou, *J. Am. Chem. Soc.*, 2011, **133**, 19314-19317.
12. G. F. Ortiz, I. Hanzu, T. Djenizian, P. Lavela, J. L. Tirado and P. Knauth, *Chem. Mater.*, 2008, **21**, 63-67.
13. C. K. Chan, H. Peng, G. Liu, K. McIlwrath, X. F. Zhang, R. A. Huggins and Y. Cui, *Nat. Nano.*, 2008, **3**, 31-35.
14. L.-F. Cui, R. Ruffo, C. K. Chan, H. Peng and Y. Cui, *Nano Lett.*, 2008, **9**, 491-495.
15. X. Xiao, L. Yang, H. Zhao, Z. Hu and Y. Li, *Nano Res.*, 2012, **5**, 27-32.
16. H. B. Wu, J. S. Chen, H. H. Hng and X. Wen Lou, *Nanoscale*, 2012, **4**, 2526-2542.
17. L. Zhang, G. Zhang, H. B. Wu, L. Yu and X. W. Lou, *Adv. Mater.*, 2013, **25**, 2589-2593.
18. S. Xin, Y.-G. Guo and L.-J. Wan, *Acc. Chem. Res.*, 2012, **45**, 1759-1769.
19. X. Liu, M. Wu, M. Li, X. Pan, J. Chen and X. Bao, *J. Mater. Chem. A*, 2013, **1**, 9527-9535.
20. H.-G. Jung, S.-T. Myung, C. S. Yoon, S.-B. Son, K. H. Oh, K. Amine, B. Scrosati and Y.-K. Sun, *Energy & Environ. Sci.*, 2011, **4**, 1345-1351.
21. X. Sun and Y. Li, *Angew. Chem. Int. Ed.*, 2004, **43**, 597-601.
22. X. Sun and Y. Li, *Langmuir*, 2005, **21**, 6019-6024.
23. X. Sun, J. Liu and Y. Li, *Chem. Mater.*, 2006, **18**, 3486-3494.
24. C. Wang, Z.-X. Deng and Y. Li, *Inorg. Chem.*, 2001, **40**, 5210-5214.
25. J. Zhang, M. Li, Z. Feng, J. Chen and C. Li, *The Journal of Physical Chemistry B*, 2005, **110**, 927-935.
26. G. S. Chai, S. B. Yoon, J.-S. Yu, J.-H. Choi and Y.-E. Sung, *J. Phys. Chem. B*, 2004, **108**, 7074-7079.
27. X. Zhi, G. Liang, L. Wang, X. Ou, L. Gao and X. Jie, *J Alloy. Compd.*, 2010, **503**, 370-374.
28. M. Sevilla and A. B. Fuertes, *Carbon*, 2006, **44**, 468-474.
29. M. Wagemaker, W. J. H. Borghols and F. M. Mulder, *J. Am. Chem. Soc.*, 2007, **129**, 4323-4327.
30. J. W. Kang, D. H. Kim, V. Mathew, J. S. Lim, J. H. Gim and J. Kim, *J. Electrochem. Soc.*, 2011, **158**, A59-A62.
31. C. Jiang, M. Wei, Z. Qi, T. Kudo, I. Honma and H. Zhou, *J. Power Sources*, 2007, **166**, 239-243.
32. C. Natarajan, K. Setoguchi and G. Nogami, *Electrochim. Acta*, 1998, **43**, 3371-3374.